High-Intensity Focused Ultrasound Surgery Based on KUKA Robot

A Computer-Assisted Platform for Noninvasive Surgical Treatments on Static and Moving Organs

xxxxx

By Andrea Mariani, Laura Morchi, Alessandro Diodato, Selene Tognarelli, and Arianna Menciassi

High-intensity focused ultrasound surgery based on a KUKA robot (HIFUSK) can address unmet clinical needs in the treatment of pathological tissues, such as cancerous tissues. HIFUSK is the marriage of two technologies: robotics and focused ultrasound (FUS). Such a combination results in a surgical treatment that is precise and noninvasive (no incisions, no anesthesia, and no ionizing energy) thanks to robotics and FUS, respectively. Robotic control and machine learning algorithms ensure safety even in case of target motions during therapy. The platform has been validated in dry lab/ex vivo scenarios, and it was preliminarily tested in terms of safety and efficacy during an in vivo test on a large animal model.

FUS Surgery

Technology Overview

US consists of mechanical waves characterized by frequencies that are higher with respect to the upper audible boundary of human hearing (i.e., higher than 20 kHz). The use of US in medicine for diagnostic imaging has been well established since the second half of the past century. On the other hand, the therapeutic use of US is a domain that has ample room for research and innovation. In this scenario, FUS plays a paramount role. The FUS principle is analogous to the one of a convex lens that focuses a beam of sunlight on a single spot. If this spot lies on a piece of paper, the paper will be locally burned. In a similar way, FUS uses an acoustic lens to focus multiple beams of US on a certain target, causing a negligible effect where the individual beams pass through but resulting in a relevant amount of energy being delivered to the focal spot. If this spot is located deep in the human body, it is possible to produce a localized relevant biological effect while preserving the integrity of the surrounding tissues [1], as in Figure 1.

Medical Applications

FUS could potentially change the treatment paradigm of several medical conditions. Indeed, at low to medium acoustic intensities, FUS can be used for triggering drug delivery. Localized drug release can be activated by applying FUS on nanosized

Digital Object Identifier 10.1109/MRA.2022.3188221
Date of current version: 1 August 2022

IEEE Robotics & Automation Magazine (RAM) paper, presented at ICRA 2023, London, UK. Cite as RAM paper.

1070-9932/22©2022IEEE

carriers, such as thermosensitive liposomes [2]. In case of high amounts of energy at the focal spot (i.e., from 1 to 10 kW/cm^2) and a frequency in the range of 0.5–3 MHz, FUS is usually referred to as *high-intensity focused ultrasound* (*HIFU*) [3].

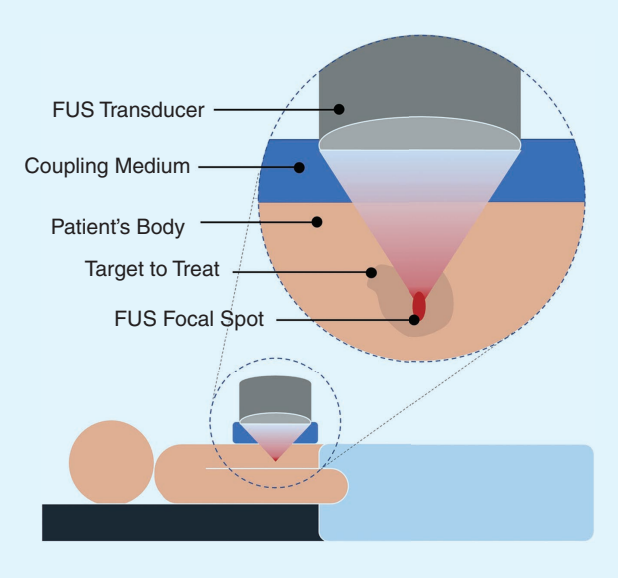

Figure 1. A medical application of FUS. A transducer generates a beam of FUS. An acoustic coupling medium guarantees the correct propagation of this beam from the therapeutic device (i.e., the FUS transducer) to the patient's inner body. The FUS beam has a negligible effect on the tissues it propagates through, except for its focal spot, where a mechanical or thermal lesion occurs. This focal spot, which can be positioned in the target to treat, typically has the size of a grain of rice.

Neurological disorders, including essential tremors, Parkinson's disease, and neuropathic pain can be approached by HIFU. In addition, new emerging applications have been recently investigated, namely, vessel blockage, to control hemorrhages, thrombolysis, and abscesses [4]. However, one of the most promising fields of HIFU application is cancer therapy. Indeed, the possibility to noninvasively—without any incision or the use of ionizing radiation—focus a high-intensity beam within the human body sets HIFU as a valid alternative to traditional cancer surgical treatments, both for benign and malignant tumors. Liver, kidney, pancreas, uterine, thyroid, bone, brain, prostate, and soft tissue malignancies can be addressed using HIFU [5]. Figure 2 reports the main anatomical sites where HIFU surgery has been applied for tumor treatment, along with the number of treatments, the state of the research, and regulatory approvals [1].

Image Guidance Techniques

The quality of HIFU treatments is strictly related to precision and accuracy in target identification as well as for the monitoring of energy deposition throughout the therapy [3]. This can be achieved by image guidance, which can be carried out by using magnetic resonance (MR) and US imaging. Excellent soft tissue contrast together with an ability to monitor HIFU-induced temperature changes make MR guidance attractive for some clinical applications. However, the integration of a HIFU therapy unit into an MR scanner is challenging, and it calls for complicated and expensive technology (e.g., the Exablate system). On the other hand, using US imaging for target identification and therapy monitoring leads to relevant advantages: 1)

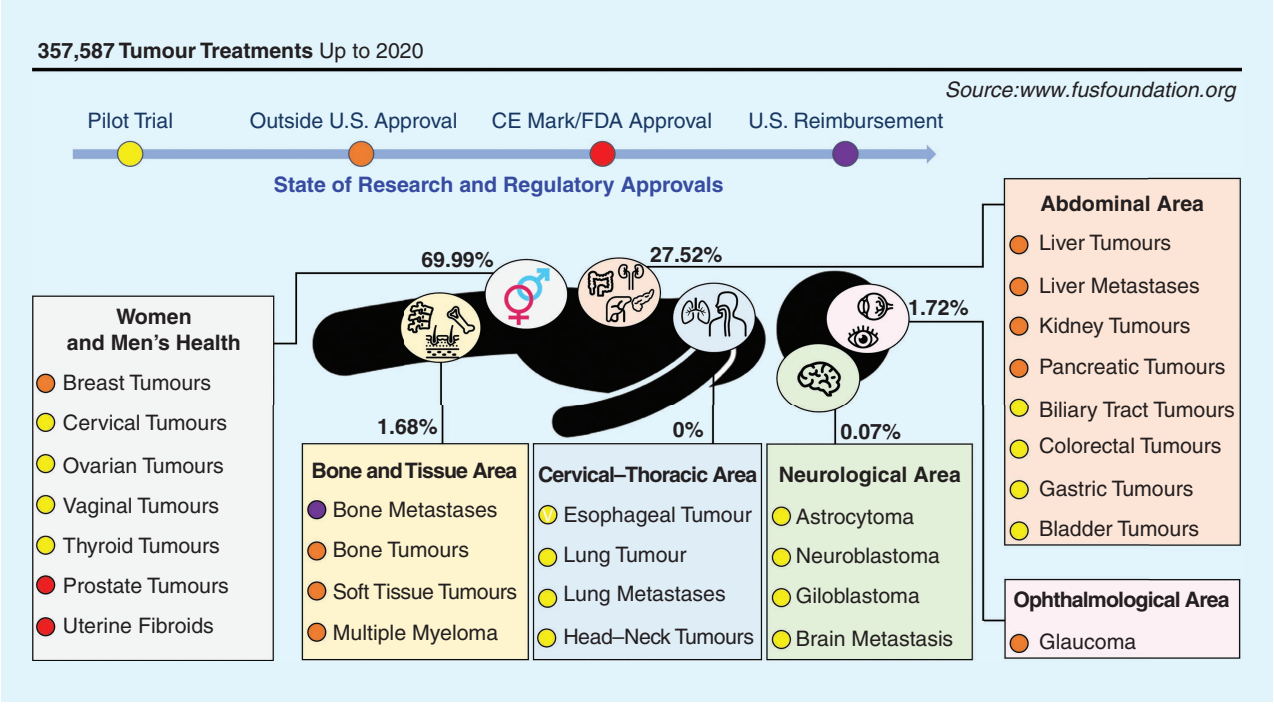

Figure 2. Tumor treatment with HIFU: an overview of the main applications. Percentages next to each area indicate how many tumor treatments were conducted with HIFU out of the total procedures (i.e., 357,587). CE: Conformitè Europëenne; FDA: Food and Drug Administration.

ease of use, 2) relatively low cost, 3) portability, and 4) wide patient access. In addition, US guidance is intrinsically safe because it enables visualizing only what can be treated (i.e., having the same acoustic window for monitoring and treatment). Additionally, it provides methods of tissue analysis (such as elastography [6]) that can be useful to assess therapeutic effects. Finally, the refresh rate of US imaging is higher if compared to MR, thus enabling online corrections to the treatment plan. With the final aim to develop a flexible platform for HIFU treatment, the US imaging modality may represent the most suitable solution both for cost and applicability.

Commercial HIFU Platforms With US Guidance

US-guided HIFU (USgHIFU) takes advantage of a US imaging probe coaxially mounted with respect to the HIFU therapeutic transducer. Currently, USgHIFU systems come with two possible designs (Figure 3). In earlier systems, the patient lies on the operating table, partially immersed in a degassed water bath. The transducer and confocal imaging probe are mounted inside the water bath. This is the case of HAIFU JC (Haifu Medical Technology) and Surround Sound Prototype (Kona Medical). Water guarantees correct acoustic coupling—and, in turn, energy transmission—between the transducer and human body. However, this configuration results in a bulky system with reduced flexibility in terms of the range of motion of the HIFU transducer. Thus, treatment planning and the number of possible treatment sites are limited.

The alternative design overcomes the described limitations by mounting the transducer on a manipulator, top-down approaching the patient, using a water-filled balloon between the transducer and patient for ensuring the correct acoustic coupling. Examples of this configuration include the Alpius 900 (Alpinion Medical Sytems) and EchoPulse (Theraclion). These platforms take advantage of a passive mechanical arm. Thus, the physician has to manually position the transducer with respect to the anatomical area to treat, reducing the precision and repeatability of the procedure as well as introducing high dependency on the operator's experience. In addition, in both platform designs, the HIFU treatment is limited to nonmoving organs, that is, organs that are not subjected to motion induced by physiological breathing and blood pressure.

The introduction of a robotic arm with active control could boost the application of HIFU for surgical treatments. Robotics could represent the enabling technology for precise and automatic targeting as well as the extension of HIFU treatment to moving organs, while adding flexibility to the therapy procedure [Figure 3(b)].

Related Research to Robotic HIFU

Although there are examples of works combining robotics with US for diagnostic purposes and for guiding the insertion of surgical tools (e.g., [7]–[9]), few research groups have tried to combine robotics and USgHIFU. Kheng et. al. [10] and Pather et al. [11] proposed a robotic device for HIFU treatment. However, the robot was intended only as a transducer holder for precise positioning. No active and image-guided control of the robotic arm was implemented. A six-degrees-of-freedom (DoF) robot coupled with a HIFU transducer was reported in [12]. In that work, an industrial robot was used to position the HIFU transducer. However, no coupling device was present, thus requiring the transducer to be immersed in water for therapy delivery.

Yonetsuji et al., in [13], developed a 4-DoF robot-assisted HIFU platform. Also in that case, no coupling device was provided, and the robot was designed to work completely immersed in water. Additionally, flexibility and dexterity were limited due to the reduced number of DoF. A 5-DoF parallel link robotic HIFU system was proposed by Tang et al. [14]. The system was designed for breast treatments, and it enabled 3D US image reconstruction, target segmentation, treatment path generation, and automatic HIFU irradiation. No coupling device was presented, and an underwater workspace was designed for therapy delivery, thus potentially limiting patient comfort and system flexibility. A robot-assisted HIFU system for the treatment of peripheral artery disease was reported in [15], yet the robotic arm was simply used as a static holder.

However, in all the previous studies, no tracking strategy to enable the treatment of moving organs was implemented. Koizumi et al., in [16], reported a USgHIFU system that compensated for motion by tracking and following the area to be treated by stereo US imaging. The transducer was completely immersed in water, and it was moved by a motorized slide, thus limiting the flexibility of therapy delivery. Chanel et al., in [17], described the only robotic USgHIFU system for real-time compensation for intra-abdominal organ motion by US visual servoing. However, this strategy was able to compensate for only 82.6% of the breathing-induced motion, and it neglected the patient–transducer coupling during motion compensation. An et al. [18] introduced a US imaging-assisted robotic HIFU ablation system with a displacement compensatory mechanism. Target motion compensation was based on a correlative polynomial function between the heaving chest position, recorded using an optical tracker, and the tumor position, recorded using US imaging. However, this strategy showed a compensation error of 1.72 ± 1.26 mm. In addition, the robotic arm was a 4-DoF manipulator, and the system was designed to be fully immersed in water, thus reducing patient comfort and system dexterity and flexibility.

Objective of This Work

This literature overview highlights the lack of a robot-assisted HIFU platform that takes real advantage of robotics to cover all the limitations of the currently available HIFU systems. In this direction, some years ago, we introduced the Focused Ultrasound Therapy Using Robotic Approaches (FUTURA) platform [19]. This platform combines two independent robotic manipulators, one for therapy delivery and one for therapy guidance. Starting from that experience and with the aim to improve platform usability, cost-effectiveness, and portability, we introduce the HIFUSK platform. HIFUSK

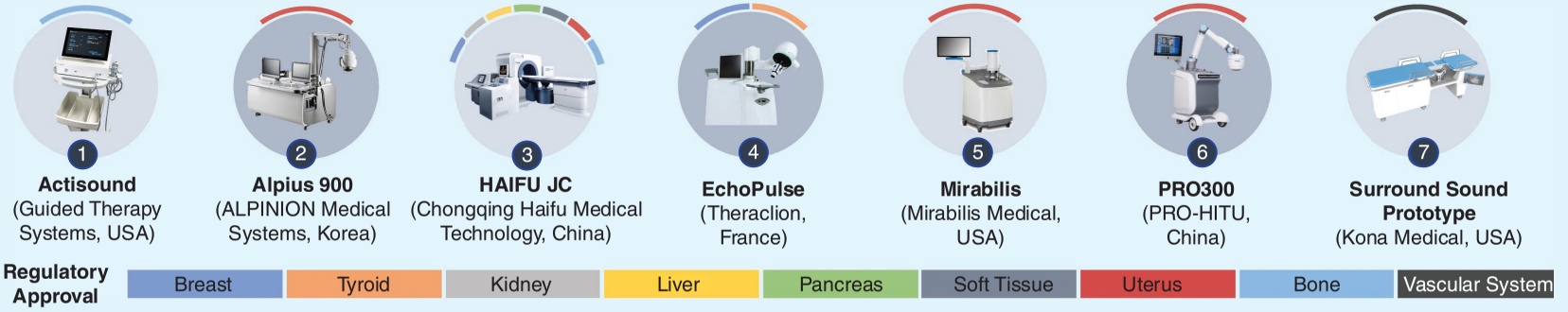

(a)

Limitation	What Does It Mean	Who Is Affected	Robotic Solution, Such as HIFUSK	
Lack of Flexibility	The device is specific for one or a few clinical targets.	1 2 4 5 6 7	Multiple Targets	Robotic positioning of the HIFU transducer with respect to the patient.
Static Targets	The technique can be applied mainly on nonmoving organs, or in some cases on moving targets but in combination with respiratory gating or some form of breath hold.	1 2 3 4 5 6 7	Moving Targets	Image-based tracking and robot-assisted motion compensation.
Long Treatment	Treatments are not automated, and therefore the total duration of the procedure is long (e.g., few hours).	3 4 5 7	Quicker Treatment	Automatization of the procedure by robotic guidance.
Uncomfortable Setup	Positioning of the patient is inconvenient and difficult, also limiting the medical team.	3 7	Handy	Robot-assisted positioning of the HIFU transducer and optimized coupling with the patient.
Encumbrance	The device is large and heavy, requiring special equipment and arrangement of the operating room.	3 7	Plug and Play	Lightweight robotic arm with proper workspace.

(b)

Figure 3. (a) The USgHIFU platforms currently available on the noninvasive HIFU therapy market and the anatomical targets for which they received regulatory approval. (b) The platforms' major limitations and how a robot-assisted solution, such as HIFUSK, can overcome the shortfalls.

combines the HIFU technology developed in FUTURA with the KUKA LBR medical robot (LBR Med 14 R820), the only robotic arm available on the market that is certified for clinical applications. The aim of this work is to develop and extensively validate a HIFU platform with robotic control and US imaging guidance to address both static and moving organs through a dedicated motion tracking technique. A specific focus on strategies to ensure patient safety throughout the treatment is also key: in this regard, dedicated components of the HIFUSK platform are presented and discussed in this work.

Design and Implementation of HIFUSK

This section first illustrates the HIFUSK platform in terms of its components. Then, the description focuses on the system's key functionalities as a robot-assisted surgical platform for FUS treatment of both static and moving organs in the abdominal area.

Hardware Modules

The HIFUSK components are presented in Figure 4(a). HIFUSK is based on a 7-DoF robotic arm. In all its seven axes, the LBR Med is equipped with joint torque sensors that enable the detection of applied forces. The robotic arm mounts the therapeutic HIFU transducer. This is a 16-channel phased annular array transducer with a central frequency of 1.2 MHz, diameter of 120 mm, and focal length of 120 mm (produced by Imasonic). The focal length can be further adjusted by applying electronic axial steering in the range ±20 mm, thus obtaining a focal length in the interval of 100–140 mm. The HIFU transducer is driven by a 16-channel high-power signal generator (Image Guided Therapy). Each channel can reach up to 20 W, thus generating a maximum power of 320 W.

To guide the therapy, a 2D linear phased-array US probe, with a 4–7-MHz bandwidth (Analogic Ultrasound), is

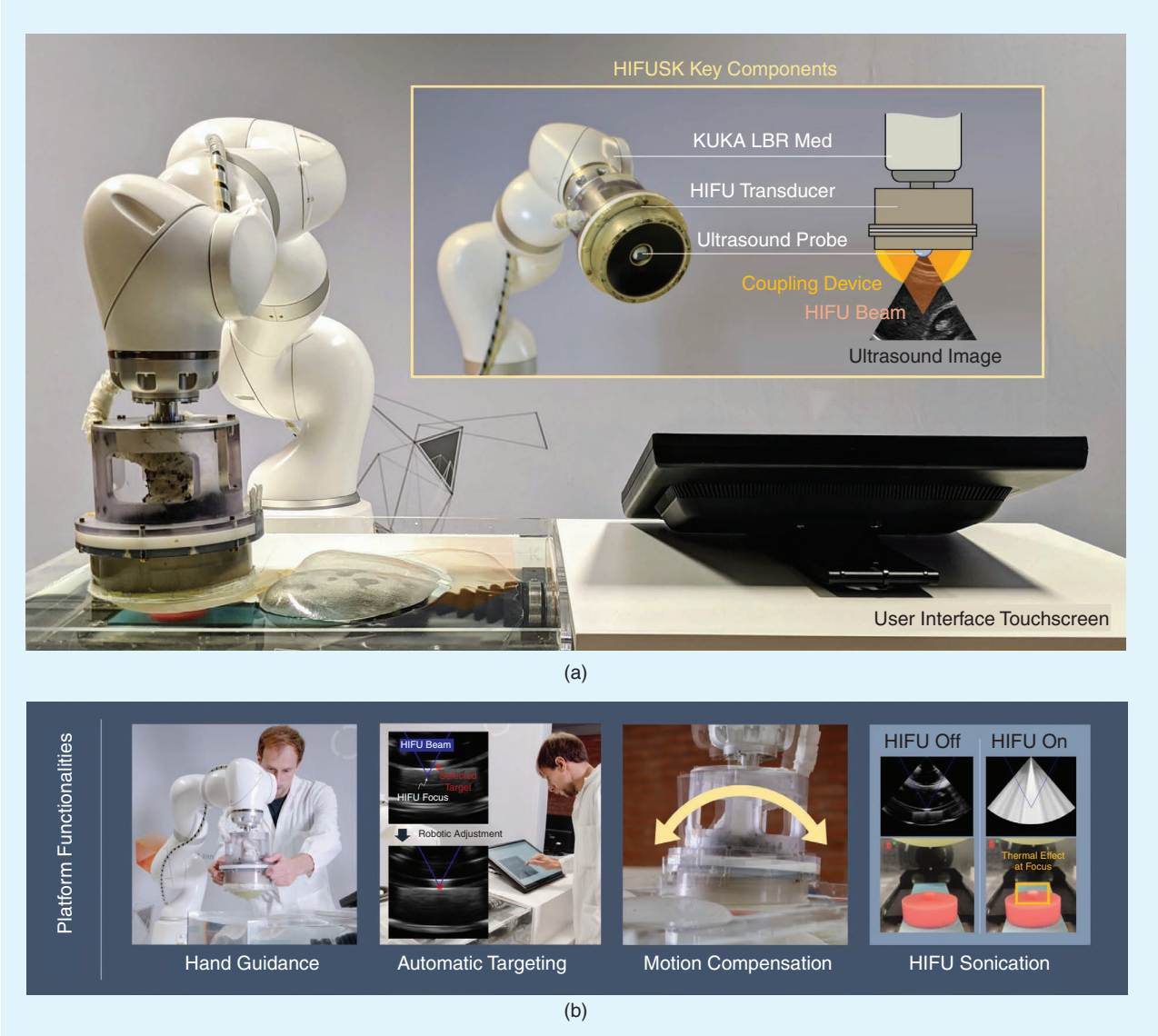

Figure 4. The (a) HIFUSK platform components and (b) functionalities.

confocally mounted on the HIFU transducer. A research US system is connected to the US probe for common B-mode US image acquisition, system parameter selection, and recording of raw radio frequency data. This final operation is essential for further imaging analysis and the implementation of image-based algorithms.

The acoustic coupling between the HIFU transducer and patient body is ensured by a balloon made with a flexible latex membrane (150 μm in thickness). The balloon is attached to the HIFU transducer and filled with degassed water. Water is continuously recirculated through a degassing circuit to avoid cavitation effects due to the possible presence of air particles inside the water-filled balloon while preventing excessive heating of the balloon itself.

Finally, HIFUSK is equipped with dedicated software (see the "Software Architecture" section) running on an Intel Core i7-9700, 3-GHz computer with a NVIDIA GeForce RTX 2070 SUPER video card for synchronization and data exchange among the different platform components. A touchscreen monitor (FLATRON 19MB15T-B; LG Electronics) is used to provide the operator with a GUI.

Software Modules

This section illustrates the modules of the HIFUSK platform as functionalities that enable robot-assisted FUS treatment. These functionalities, together with their methodological details, are described in the order in which they would be used by the physician throughout the treatment. A video showing a demonstration of the HIFUSK platform can be found as a multimedia attachment (available at https://doi.org/10.1109/MRA.2022.3188221). The safety measures implemented in the HIFUSK platform will also be discussed.

HIFUSK Functionalities

A GUI allows the physician to visualize the US images and enable the functionality required at each step of the treatment. The functionalities are as follows:

1) *Hand guidance*: At the beginning of the surgical procedure, the HIFU transducer has to be positioned in contact with the patient's skin. This step is carried out by the robot-assisted hand guidance of the transducer. A button located on the HIFU transducer enables the unlocking of the robotic arm and movement of the therapeutic device. Once this coupling is completed (i.e., the coupling balloon is in contact with the patient's skin), the clinician begins visualizing the inner anatomical structures of the patient on the images from the confocal US probe. Further hand guidance enables the identification of the target where the HIFU sonication is to be performed.
2) *Automatic targeting*: The HIFUSK platform allows the physician to manually select the target on the echographic images visualized in the GUI. The physician can freeze the image and tap the screen to select the target, which will appear as a visual overlay (a red dot) on the image. The robot pose is computed to have a match between the focus of the HIFU transducer and the target. Before enabling robot motion, a check on the motion amplitude is conducted (see the "HIFUSK Safety Measures" section). Then, the robot automatically adjusts its pose. This adjustment is performed as a translation in the US imaging plane. This translation (${}^{rb}\Delta$) is computed as

$$ {}^{\text{rb}}\Delta = {}^{\text{rb}}T_{\text{ee}} * ({}^{\text{ee}}T_{\text{im}} * k * {}^{\text{im}}t - {}^{\text{ee}}T_{\text{hifu}}\,{}^{\text{hifu}}f), \tag{1} $$

where ${}^{\text{rb}}T_{\text{ee}}$ is the robot forward kinematics; ${}^{\text{ee}}T_{\text{im}}$ and ${}^{\text{ee}}T_{\text{hifu}}$ are the transformations from the imaging and HIFU reference frames (RFs), respectively, to the end effector RF (both estimated from the system CAD model); ${}^{\text{im}}t$ is the selected target in the echographic imaging RF; k is the pixel-to-meter conversion factor; and ${}^{\text{hifu}}f$ is the HIFU focus in the HIFU transducer RF. Figure 5 presents these RFs and points for further clarification.
3) *Motion compensation*: Organs in the abdominal area (such as the liver, kidneys, and pancreas) are subjected to motion

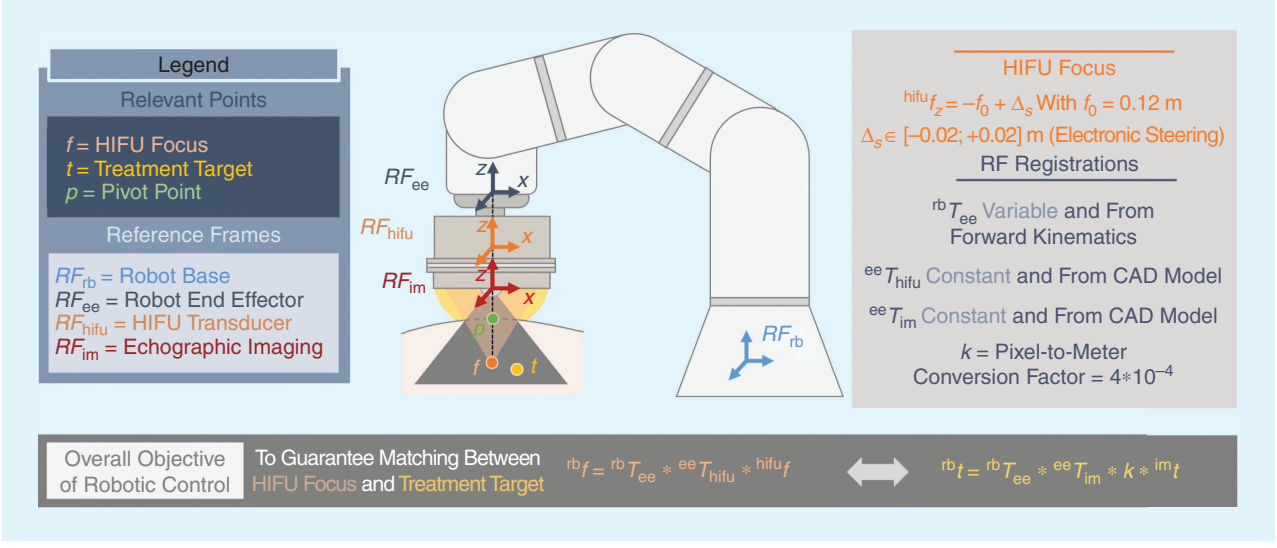

Figure 5. The HIFUSK platform in terms of relevant RFs, salient points throughout the treatment, and system parameters.

due mainly to physiological breathing. This motion is typically periodic in time (with breathing frequency usually between 0.2 and 0.3 Hz) and linear in space (up to 2 cm) [20]. As a drawback, this can either cause lesions on undesired targets or reduce treatment efficiency. The HIFUSK platform exploits robotic control and machine learning to track and compensate for target motions. The physician can select a region of interest (ROI) in the echographic images of the area surrounding the target defined in step 2. This ROI is tracked in the subsequent images, and its motion is learned for controlling the robot and keeping the HIFU focus where the target is estimated to be. The motion compensation embedded in the HIFUSK platform stems from a previous work of the authors [21]. Specifically, the HIFUSK motion compensation functionality encompasses three subblocks (Figure 6): the image-based tracking, the trajectory learning, and the robotic control, described as follows:

- The image-based tracking detects the ROI, which was selected by the physician together with the target, across the new images from the US probe. This tracking is based on the Tracking–Learning–Detection (TLD) algorithm [22], which is suited for frame-to-frame, long-term tracking of unknown objects. Additionally, TLD is capable of adapting to changes in the appearance of the target region, and it features robustness to false positives. Thus, it fits our purpose of tracking a target area on B-mode US images during HIFU treatments. The trajectory of the ROI barycenter [$^{im}\overline{ROI}(n)$, where n is the time sample] is mapped on the target selected by the physician so that the target coordinates [$^{im}\bar{t}(n)$] in each frame are identified. This is accomplished by assuming a rigid transformation ($^{im}\Delta_{ROI-t}$) between the target and ROI barycenter in the imaging frame at the physician's selection. Finally, the target trajectory is reported in the robot base RF [$^{rb}\bar{t}(n)$].
- The trajectory learning takes as an input the target trajectory [$^{rb}\bar{t}(n)$], and it estimates its periodic motion [$^{rb}\tilde{t}(n)$]. This prediction is required to consider the delay in the robot control (in our platform, it is estimated as 100 ms). The trajectory learning is achieved by using windowed sinusoidal regression: after each time window (3s), sinusoidal regression is performed on the three components (x, y, and z) of $^{rb}\bar{t}(n)$, considering all the points from the latest three-time windows (i.e., $n \in [t_{now} - 9\text{ s}, t_{now}]$).
- The robotic control enables compensating for the estimated motion of the target. This is performed by

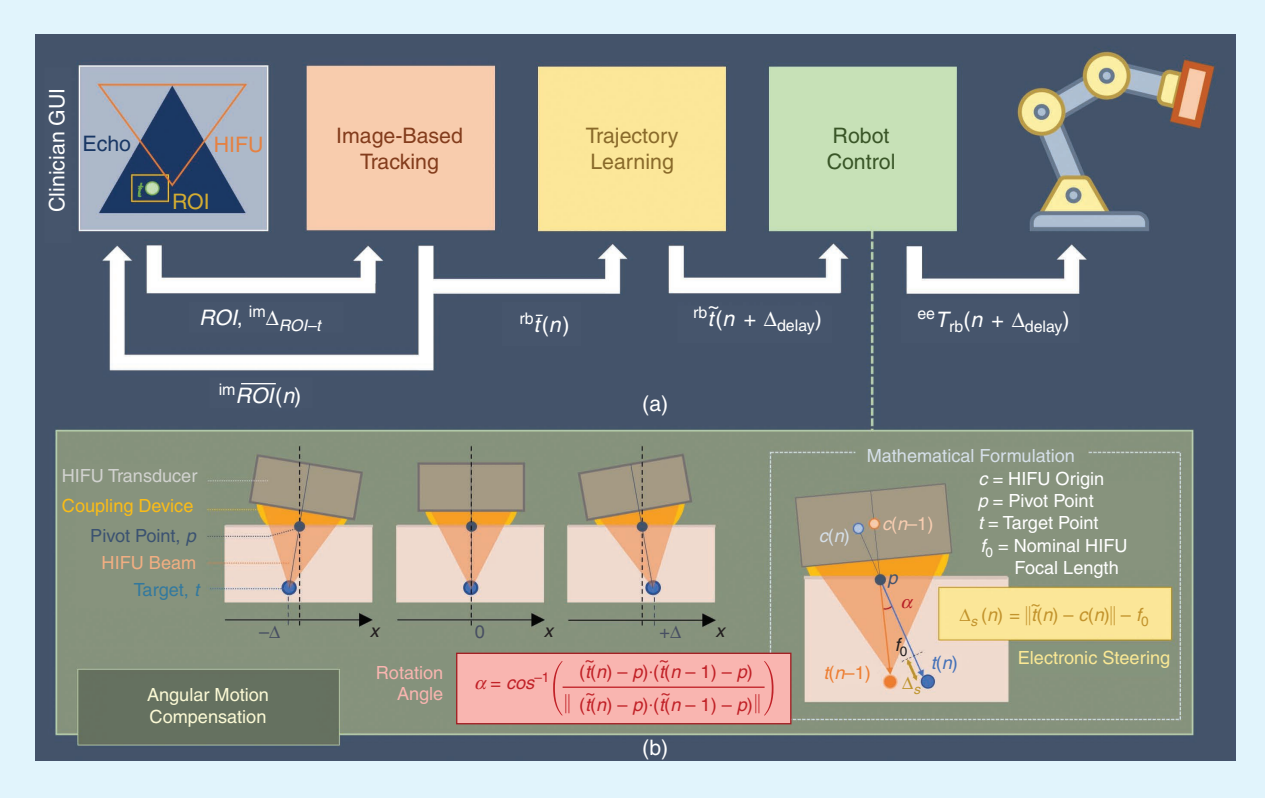

Figure 6. The architecture of the HIFUSK motion compensation functionality. (a) The physician selects the target (t) and a surrounding ROI in a frozen echographic image. Then, $^{im}\Delta_{ROI-t}$ defines the rigid transformation between the ROI barycenter and target in the imaging frame (*im*). The image-based tracking finds that ROI in the following images. At any sample n, this $^{im}\overline{ROI}(n)$ is provided back to the GUI for the physician's visual inspection, and it is converted in target position $^{rb}\bar{t}(n)$ in the robot base (*rb*) RF. This trajectory is later estimated as $^{rb}\tilde{t}(n)$ by sinus interpolation. This estimation (together with the control delay, Δ_{delay}, i.e., 100 ms) is used to define the robot pose $^{ee}T_{rb}(n + \Delta_{delay})$ for motion compensation. (b) The robot rotates the HIFU transducer and attached coupling device around a pivotal point (p), and the electronic steering (Δ_s) of the HIFU beam is applied to match the target (t).

rotating the HIFU transducer around a virtual pivot point (p), while the focal depth ($^{\text{hifu}}f$) is continuously adjusted thanks to the axial electronic steering capabilities of the HIFU transducer. By keeping the same contact point between the transducer and the patient's skin (i.e., the virtual pivot point), variations in the acoustic window are minimized. Specifically, the HIFU transducer is rotated at an angle α around the axis v passing through the pivot point p and normal to the imaging plane. Such an angle is computed as

$$\alpha = \cos^{-1}\left(\frac{(^{\text{rb}}\tilde{t}(n) - {}^{\text{rb}}p)\cdot(^{\text{rb}}\tilde{t}(n-1) - {}^{\text{rb}}p)}{(^{\text{rb}}\tilde{t}(n) - {}^{\text{rb}}p)\cdot(^{\text{rb}}\tilde{t}(n-1) - {}^{\text{rb}}p)}\right), \quad (2)$$

where $^{\text{rb}}\tilde{t}(n-1)$ and $^{\text{rb}}\tilde{t}(n)$ are the estimated target positions in the robot base RF at time $n-1$ and n, respectively, and $^{\text{rb}}p$ is the pivot point in the robot base RF. This point $^{\text{rb}}p$ is defined as

$$^{\text{rb}}p = {}^{\text{rb}}c(n) + [0; 0; \Delta_{\text{balloon}}], \quad (3)$$

where $^{\text{rb}}c(n)$ is the HIFU origin in the robot base RF (that is available from the robot forward kinematics $^{\text{rb}}T_{\text{ee}}$ and registration $^{\text{ee}}T_{\text{hifu}}$) and Δ_{balloon} is equal to 0.05 m (to take into account the encumbrance of the coupling balloon). Additionally, the electronic steering Δ_s of the HIFU beam is applied as

$$\Delta_s = \left\| {}^{\text{rb}}\tilde{t}(n) - {}^{\text{rb}}c(n) \right\| - f_0, \quad (4)$$

where $^{\text{rb}}\tilde{t}(n)$ is the estimated target position in the robot base RF at time n, $^{\text{rb}}c(n)$ is the HIFU origin in the robot base RF, and f_0 is the nominal focal length of the HIFU transducer (i.e., 0.12 m).

4) *HIFU sonication*: In static and motion-compensated conditions, the acoustic coupling between the HIFU transducer and patient is checked before enabling HIFU sonication (see the "HIFUSK Safety Measures" section). Afterward, treatment can be performed. Sonication parameters, i.e., intensity, duration, and duty cycle, can be selected through the GUI to produce a thermal and/or mechanical effect on the target [23]. After the physician's acknowledgment, the HIFU sonication is executed.

HIFUSK Safety Measures

The following measures were implemented to verify the safety of the full procedure, i.e., the global safety (GS), as well as during specific steps of the treatment, i.e., functionality-specific safety (FS):

- *GS (force monitoring)*: The interaction force between the transducer and patient (or in general, the external environment) is checked throughout the full procedure. This verifies that this force falls into the safety interval for the patient's body, namely, lower than 9 N [24].
- *GS (emergency button)*: The physician always has supervision over the procedure: he or she can stop the robot motion and HIFU sonication by pressing an emergency button on the GUI.
- *FS (motion amplitude during automatic targeting)*: Before enabling the motion of the robot for matching the focus of the HIFU transducer with the selected target, verification of the motion amplitude is conducted. This step aims at avoiding the loss of the acoustic window and coupling after this adjustment. A safety threshold is set on the robot translation $^{\text{rb}}\Delta$ by imposing its norm to be lower than 3 cm. If this condition is not met, a popup will appear on the GUI to inform the physician that the selected target is not reachable in the current robot pose. The physician can either reselect the target or reposition the robot by using the hand guidance functionality.
- *FS (tracking error monitoring)*: A safety mechanism continuously estimates the error between the available target position, $^{\text{rb}}\bar{t}(n)$, from the image-based tracking and the one estimated by trajectory learning, $^{\text{rb}}\tilde{t}(n)$. If this error is unacceptably larger than a user-defined threshold (in our study, 2.5 mm), the HIFU sonication functionality is disabled.
- *FS (acoustic coupling verification before sonication)*: The verification of the coupling between the HIFU transducer and patient's body is a necessary step for enabling HIFU sonication. This is carried out by analyzing the radio frequency data recorded by the confocal imaging probe during a safe (i.e., 1 W in power and 1 s in duration) HIFU sonication before the actual sonication, as described in a previous work [25].

Software Architecture

This section provides a description of the overall software architecture of the HIFUSK platform. The different modules of the HIFUSK platform are controlled through dedicated software developed in the Robot Operating System (ROS) framework. Specifically, HIFUSK encompasses the following six ROS nodes:

1) *GUI node*: This was developed using Qt Creator.
2) *Robot control node*: This involves a User Datagram Protocol connection with the KUKA controller to trigger the robot control states (hand guidance, position and force control, and the brake). The KUKA controller runs an application implemented with the KUKA Sunrise operating system.
3) *Echographic imaging node*: This involves an ROS bridge with the echographic probe, using the Open Image-Guided Therapy Link protocol to stream the 500 × 500-pixel B-mode US images as an ROS topic at 30 Hz.
4) *Image-based tracking node*: This uses an open source ROS version of the OpenTLD tracker and provides continuous tracking at 20 Hz on the US images (which is adequate to track 0.2–0.3-Hz breath-induced motions).
5) *Trajectory learning node*: This uses the Python package *optimize.curve_fit* to perform sinusoidal regression.
6) *HIFU sonication node*: This involves a TCP/IP connection to direct the HIFU transducer and sonication parameters.

Validation of HIFUSK

This section describes the tests carried out to validate the HIFUSK platform. This validation moved from controlled laboratory conditions (when testing the technology on phantoms and ex vivo animal tissues) to an in vivo clinical trial on a pig.

Dry Lab Validation

We first evaluated the HIFUSK platform in a dry lab (i.e., on phantoms) in terms of motion tracking and sonication accuracy.

Experimental Setup

The experimental setup to achieve this goal is illustrated in Figure 7(a). Tests were conducted on a thermochromic silicone-based phantom [15]: the phantom changes its color according to temperature. Specifically, it turns white from red when the local temperature exceeds 65 °C. This condition can be achieved by thermal sonication. When the HIFU sonication stops, the phantom cools down and recovers the original red color. The phantom was designed in a cylindrical shape with a central peg (1 cm in radius) as a shooting target. It was attached to an acoustic absorber that was connected to a 1-DoF motorized slide. The slide simulated the motion due to respiration that has to be compensated throughout HIFU therapy. Then, the motorized slide performed a breathing-like sinusoidal motion with an amplitude of 10 mm and a frequency of 0.2 Hz (i.e., 12 breaths per minute). All the setup elements were immersed in a tank containing degassed water.

Motion Tracking and Learning Analysis

Experimental Protocol

The results of the motion compensation experiments were evaluated by comparing the target position from the encoder of the motorized slide and the one estimated from the tracking and learning modules. The target (i.e., the centroid of the phantom peg) and a surrounding ROI were selected on the user interface. The estimation of the target position from the tracking and learning modules was observed for 10 s (after the initialization of each module). This procedure was iterated 10 times.

Results

Figure 7(b) displays the target position estimated by the tracking module (red) and learning module (blue) together with the signal from the motorized slide. Both the average error and the maximum error across each repetition were computed. The average error was always less than 1 mm for each repetition. The average error from the learning module was lower with respect to the one from the tracking module, although it was characterized by higher variability across repetitions. In terms of the maximum error, the learning module featured lower values with respect to tracking, and it facilitated keeping the median maximum error around 1.6 mm.

Sonication Accuracy Analysis

Experimental Protocol

The accuracy in performing HIFU sonication was evaluated both in static and dynamic conditions, namely, simulating the target motion due to breathing. The experimental protocol included the execution of a 60-W, 10-s, continuous HIFU sonication [26]. Through the GUI, the centroid of the thermochromic phantom peg was selected as the shooting target. During sonication, a 4K, 2,160-pixel, 30 frames-per-second video was simultaneously recorded. Ten repetitions were performed. A semiautomatic video segmentation algorithm was implemented in MATLAB [Figure 7(c)]. For each repetition, the shooting accuracy was evaluated by computing the error between the selected target (i.e., the peg centroid) and actual centroid of the produced white lesion on the peg. For each video frame, segmentation was applied to extract the phantom peg and identify its centroid (p_x, p_y). Second, red–green–blue (RGB) histograms were obtained, and based on a selected RGB threshold, the white lesion was automatically extracted, and its centroid (l_x, l_y) and area were computed. The sonication error was computed as the Euclidean distance between the peg centroid and lesion centroid.

Results

Figure 7(c) reports the mean error and maximum lesion area in both static and dynamic conditions. The obtained error was lower than 0.5 mm in both cases. Although a slightly higher median value could be observed in the dynamic case (0.44 mm versus 0.32 mm in the static case), the accuracy of the HIFUSK platform resulted in adequate for HIFU applications [27]. At the same time, the maximum area of the lesion was comparable between static and dynamic conditions, with a higher median value in the dynamic one (171.7 mm^2 versus 168.9 mm^2 in the static condition).

Ex Vivo Validation

The HIFUSK platform was later tested in terms of its ability to perform thermal ablation in a more realistic environment, specifically, on ex vivo animal tissue.

Experimental Setup

Figure 8(a) shows the cylindrical (22.1 mm in diameter and 20 mm in height) 10 chicken breast samples that were used to perform HIFU sonication in the two analyzed conditions (i.e., static and dynamic). The breast samples were positioned inside a cylindrical, plastic, multiwell plate. The well plate had an opening in the bottom to avoid wave reflection.

Thermal Ablation

Experimental Protocol

For each test, the center of the sample was selected as the target through the HIFUSK GUI. The HIFU lesion parameters—intensity, duration, and duty cycle—were set at 156 W, 10 s, and 90%, respectively, to obtain a thermal lesion [23].

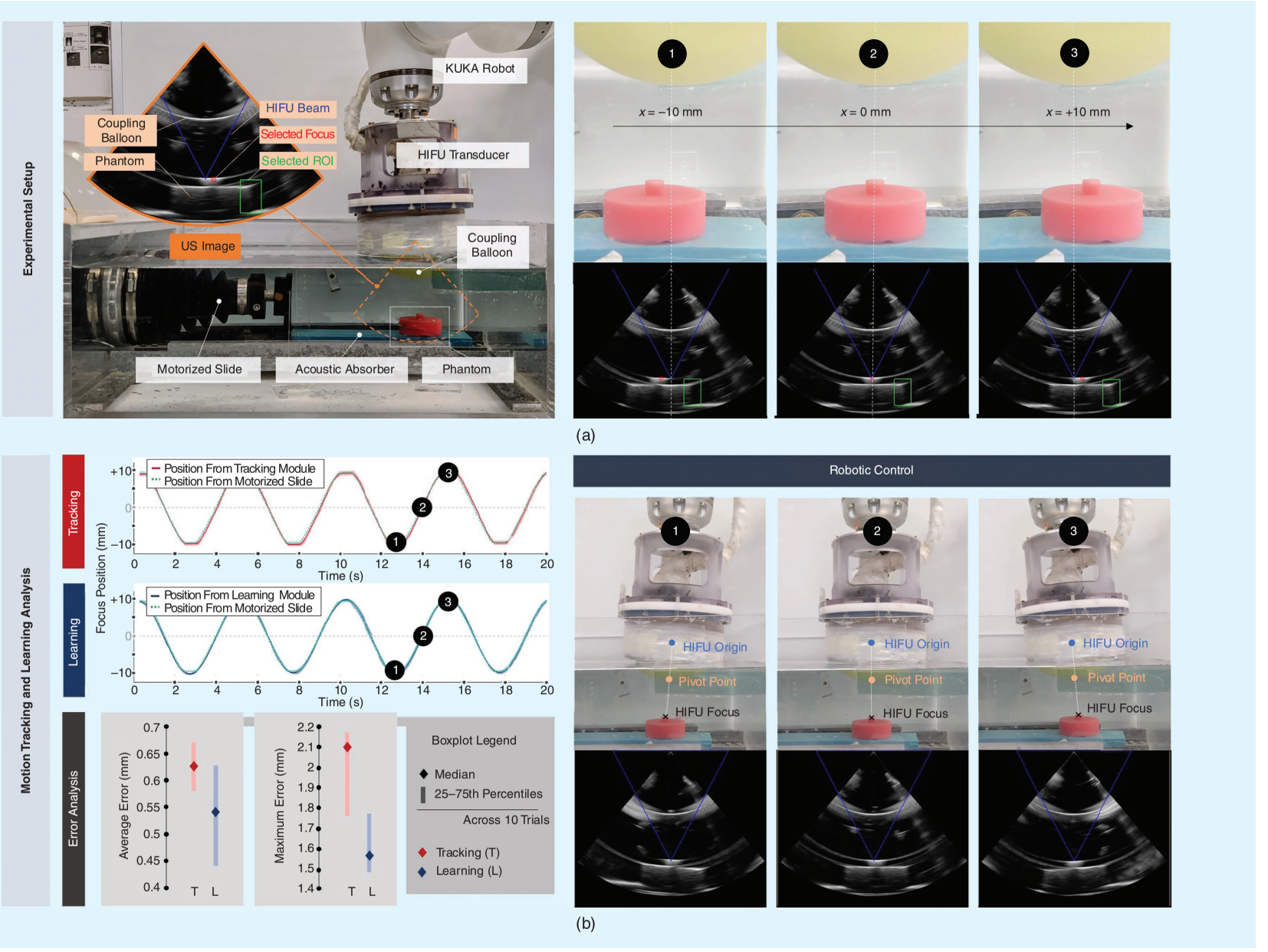

Figure 7. The dry lab validation. (a) The overall experimental setup. (b) The motion tracking and learning. The left side shows the error analysis, while the right side shows the motion compensation in terms of the robot control and its effect on the echographic images. (*Continued*)

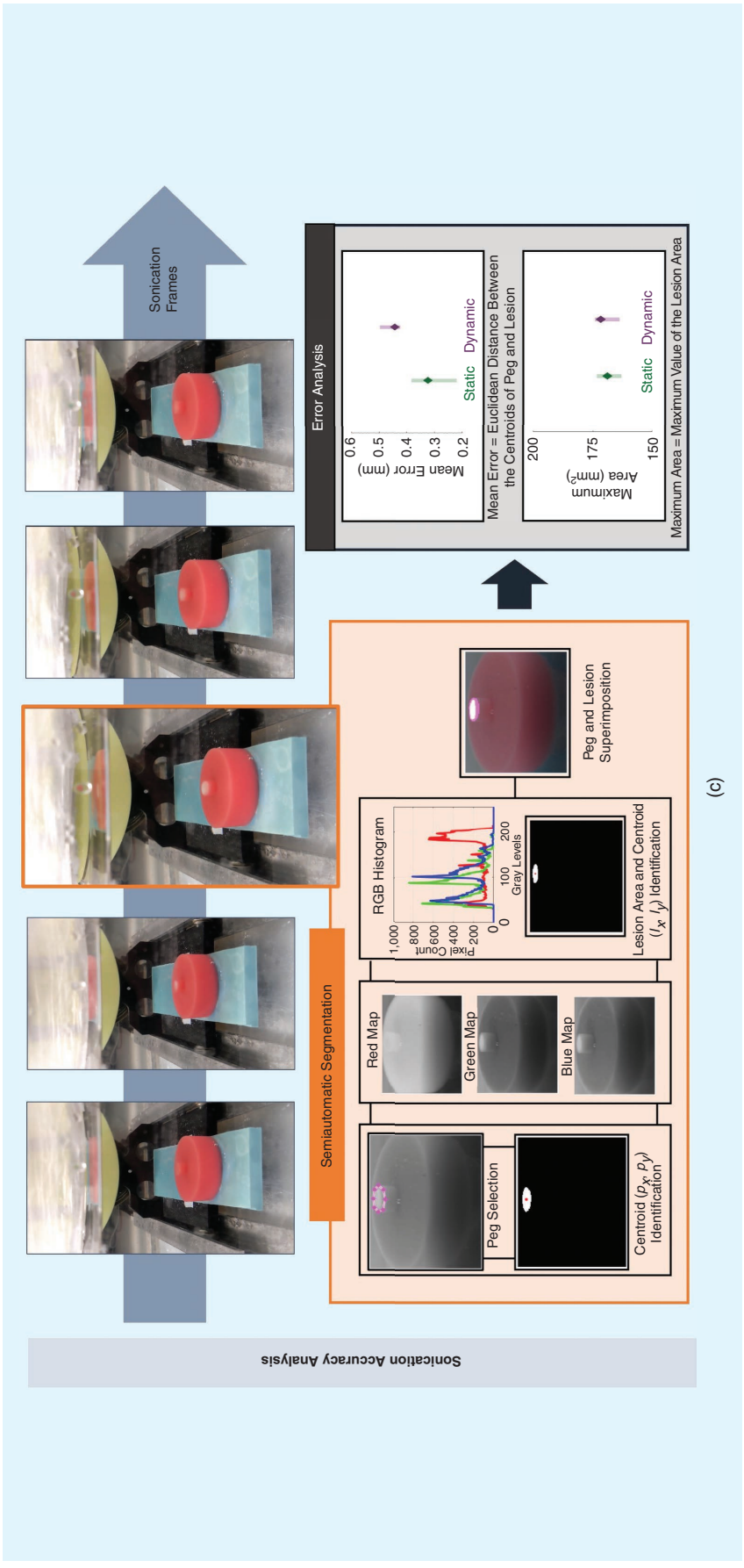

Figure 7. *(Continued)* (c) The sonication accuracy. A visual explanation of the algorithm used to segment the produced sonication in red–green–blue (RGB) images is on the left, and the error analysis is on the right.

Sonication was executed, and the sample was then sectioned to measure the lesion length (D) and width (d) with a digital caliper (0.01-mm resolution; RS Components). The volume (V) of the generated cigar-shaped lesion was computed according to (5), approximating it with a symmetrical ellipsoid:

$$V = \frac{4}{3}\pi d^2 D. \qquad (5).$$

Results

Figure 8 conveys the median value of the thermal lesion width (d), length (D), and volume (V) in static and dynamic conditions. Although slightly higher data variability can be noticed in the dynamic case, high similarity can be appreciated between the results obtained in the static condition and in the dynamic condition, where the motion compensation algorithm was applied. Due to the low number of analyzed samples, the data were compared using the nonparametric Wilcoxon rank sum test. No statistically significant difference was found between the static and dynamic cases for all three parameters (d, D, and V). Thus, the accuracy of the implemented motion compensation strategy was demonstrated on ex vivo tissue, confirming the HIFUSK platform's capability of thermally ablating static and dynamic targets.

In Vivo Validation

A first in vivo experiment was conducted on a porcine model that well resembled human anatomy and pathophysiology [28]. This in vivo testing aimed at demonstrating 1) the HIFUSK platform's usability in a clinical environment, 2) the platform's ability to perform tracking on real moving organs, and 3) the safety and efficacy in performing USgHIFU treatments in vivo by using a robotic platform.

The protocol for in vivo preclinical studies was approved by the Italian Ethical Committee in May 2020 (protocol 65E5B.48; authorization 434/2020-PR).

Experimental Setup

The in vivo test was conducted at the "Centro di Biomedicina e Sperimentale di S. Cataldo" Animal Center, Pisa, Italy, under the supervision of a physician with experience in USgHIFU treatments and a veterinary expert to take care of the animal health conditions throughout the experiment. The liver was selected as the target organ to perform the HIFU treatment.

Usability in a Clinical Environment

In vivo tests were first performed to demonstrate the compliance of the HIFUSK platform with the operating room. The platform appeared to be easy to carry and position in a reduced space. Its footprint enabled convenient integration with the other instrumentation, which was present by default [Figure 9(a)]. In addition, the GUI proved to ensure that the physician had intuitive control of the platform and its functionalities throughout the USgHIFU treatment.

Tracking Capability on Real Moving Organs

Experimental Protocol

During the in vivo experiment, the pig's ventilation was in a controlled condition, with a respiratory rate equal to 0.25 Hz. The compensation functionalities of HIFUSK were assessed in vivo by tracking and learning the motion of a liver ROI defined by the physician [see Figure 9(b)].

Results

The estimated motion was assessed as a sinusoid with a 0.24-Hz frequency and 5.29-mm amplitude. These estimated parameters were in accordance with the ventilation control frequency and motion amplitude due to respiration that we could expect in an abdominal organ [20].

Safety and Efficacy

Experimental Protocol

Despite the similarity with humans from the anatomical and pathophysiological point of view, some features of the porcine model were not optimal for the preclinical validation of FUS treatments. Indeed, pigs have a thick rind, covered with rigid bristles, that is not comparable with human skin, thus causing the FUS beam to be potentially attenuated more than in humans. To minimize this attenuation effect, the pig rind was properly prepared by removing the superficial bristles. US gel was used for improving the coupling between the water-filled balloon of the HIFUSK and the rind of the pig.

The physician initially placed the coupling balloon in contact with the pig's rind by using the hand guidance functionality until the liver was visible in the echographic images on the GUI. Then, the physician used the interface to select a desired internal point of the liver (about 2 cm below the liver's upper

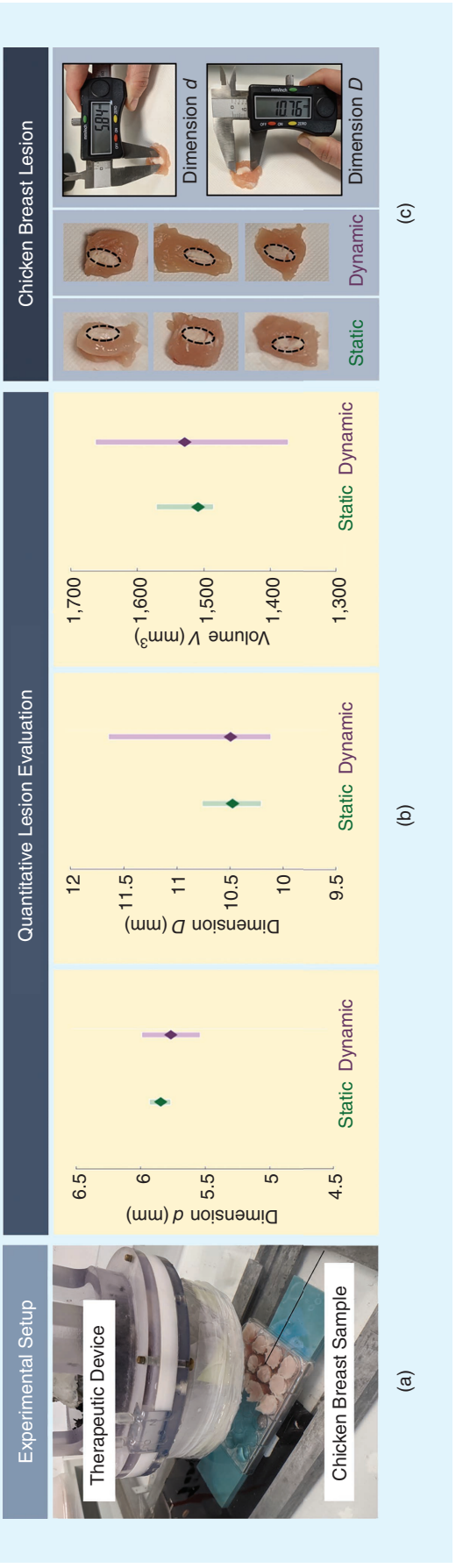

Figure 8. (a) The experimental setup used for the HIFUSK platform ex vivo validation. (b) The lesion width (*d*), length (*D*), and volume (*V*) for both static (green) and dynamic (purple) conditions. (c) The representative chicken breast thermal lesions obtained in static and dynamic conditions.

surface) as sonication target. After the robot's automatic adjustment to match the target, a single HIFU sonication (thermal ablation with parameters as in ex vivo testing) was executed. The sonication was carried out in static conditions by temporarily suppressing the pig's breathing.

To check for the safety of the performed procedure, the rind of the pig in the area where the coupling balloon was placed was analyzed by visual inspection to ensure that no burns at the coupling interface were produced. To verify the efficacy of the treatment, the liver was removed and dissected after animal suppression. The produced lesion was analyzed by means of a digital microscope (KH-7700; Hirox-USA) equipped with an MX-MACROZ IV lens (50× magnification).

Results

Results are reported in Figure 9(c). No relevant burns at the coupling interface were assessed, thus confirming the safety of the HIFUSK treatment. The produced lesion featured smaller dimensions with respect to the lesions produced in the ex vivo scenario (namely, the lesion volume was 24.8 mm^3 in vivo, while it was 1,509 mm^3 ex vivo). As mentioned, this may be caused by the thickness of the pig rind, which attenuated the HIFU beam. Therefore, a reduced quantity of energy was delivered at the focal point.

Discussion and Conclusions

HIFU surgery is a promising noninvasive and intrinsically safe therapeutic technology that could potentially change the treatment paradigm of various medical conditions, including cancer. However, the currently available systems lack flexibility in terms of therapy delivery, thus limiting the application of HIFU, especially in a delicate field such as surgery. Robotics could represent the enabling technology for HIFU treatments, accelerating the procedures' spread in clinical scenarios. Robotics can guarantee precision and automation in targeting different anatomical areas, thus speeding up the procedure and dealing with target motions. While the integration of robotics and US was previously addressed for diagnostic application, few studies reported on robot-assisted platforms for HIFU therapy, and almost none of them took advantage of active robotic control. Here, we presented the HIFUSK platform as a computer-assisted robotic platform for USgHIFU treatments on both static and moving organs. The use of a 7-DoF robotic arm improves comfort both for patients and physicians. Indeed, the patient lies on a standard operating room bed, while the target area can be easily reached thanks to the enhanced workspace of the robot.

For the first time, the design of our robot-assisted HIFU platform takes into account strategies to ensure the safety of the patient throughout the treatment (a key point for later clinical translation). Our platform was validated in both a dry lab and ex vivo scenarios, showing a HIFU sonication accuracy in line with that required in HIFU surgical procedures. Indeed, our results show a positioning accuracy of the HIFU focus always lower than 0.5 mm in both static and dynamic cases. Krafft et al. [27] reported a total positioning error of the US focus always lower than 2 mm and comparable with other existing FUS systems. This accuracy was also demonstrated while addressing a moving target, indicating a mean motion compensation error of 0.63 mm and going beyond the relative state of the art. Indeed, Chanel et al. [17] showed a 0.8-mm mean motion compensation error, while An et al., reported a mean motion compensation error of 1.72 mm [18]. However, the tracking and compensation capabilities were tested in a single direction (mainly perpendicular to the HIFU axis).

Further testing on more sophisticated phantoms will shed light on multidirectional compensation (i.e., including a

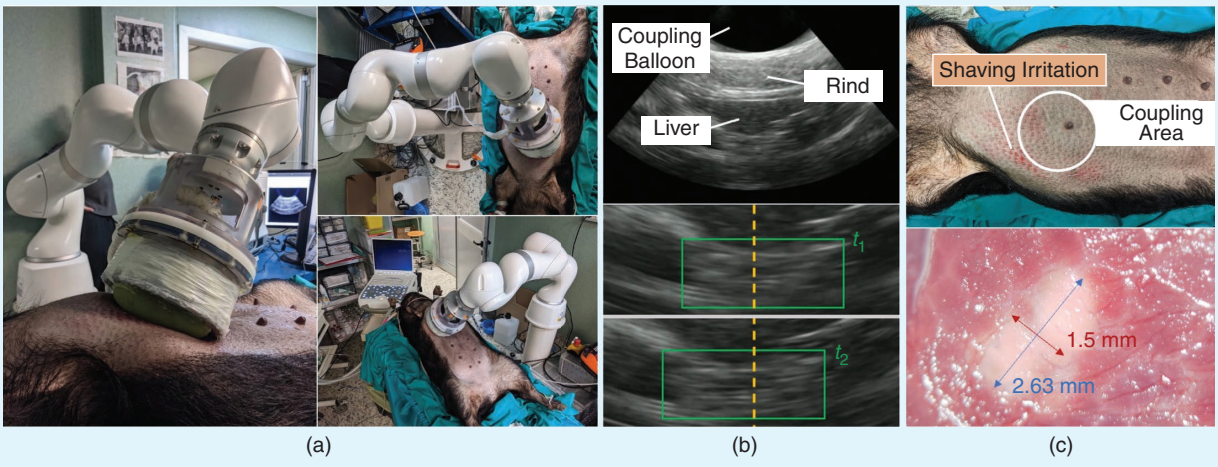

Figure 9. The HIFUSK in vivo testing. From left to right: the results associated with the platform usability, tracking capability, and treatment safety and efficacy. (a) The HIFUSK footprint enables convenient integration in the operative room. (b) (top) The US image of the target area: the HIFU transducer was coupled with the pig rind through the coupling balloon. The liver was identified as the target organ. (bottom) The physician selected an ROI (the green square) on the US image. The selected ROI at two different time instants, t_1 and t_2, respectively, is reported. (c) (top) The visual inspection of the HIFU treated area. No rind burns at the coupling interface were produced. (bottom) The digital microscope image of the lesion produced with the performed HIFU sonication.

motion component that is parallel to the HIFU axis). Additionally, all the dry lab and ex vivo tests were performed inside a water tank. The capability to keep acoustic coupling during this compensation by taking advantage of electronic axial steering and force control needs to be specifically assessed. Finally, a first in vivo experiment on a porcine model was conducted, preliminarily assessing the safety and efficacy of the proposed platform in performing a USgHIFU static treatment. Further in vivo experiments will investigate in depth the ability of HIFUSK to perform in vivo sonication during motion compensation and the possibility to treat other abdominal organs (e.g., kidneys).

In addition, a few limitations of the current system can be listed. The motion tracking and compensation rely on the physician's hand guidance to initially identify the motion plane of the target. An algorithm that automatically identifies the motion plane could improve system usability. Taking advantage of the interaction force between the HIFU transducer and the patient (which is influenced by the patient's breathing) could further improve the tracking capabilities. Additionally, the current system achieves automatic targeting through robotic assistance, yet it requires the physician to select each target (i.e., each sonication point, which is dimensionally comparable to a grain of rice). The possibility to define treatment volumes and take advantage of robotics to automatically actuate an ablation strategy could simplify the procedure and shorten the operation times. To further improve the definition of treatment volumes, the integration of a preoperative planning strategy is a plus. This strategy could be based on multimodal imaging and patient-specific models.

Acknowledgment

The HIFUSK project was the winner of the 2020 KUKA Innovation Award. We acknowledge KUKA, Augsburg, Germany, for providing us with the KUKA LBR Med robot and for technical support throughout the competition. This research was also supported by the European Commission in the framework of the FUTURA 2020 project, under grant 801451. We also acknowledge Dr. Porcelli and Prof. Di Candio, Cisanello Hospital, Pisa, Italy, for support during the in vivo clinical trial. This article has supplementary downloadable material available at https://doi.org/10.1109/MRA.2022.3188221, provided by the authors. This work involved human subjects or animals in its research. Approval of all ethical and experimental procedures and protocols was granted by the Italian Ethical Committee, May 2020, under Application No. 65E5B.48, authorization no. 434/2020-PR and performed in line with the Italian law D.lgs. 26/2014. Andrea Mariani and Laura Morchi shared first authorship and contributed equally to this work.

References

[1] "2021 state of the field." Focused Ultrasound Foundation. https://www.fusfoundation.org/images/pdf/FUSF_State_of_the_Field_2021_Final_Web.pdf (Accessed: Sep. 15, 2021).

[2] B. Kneidl, M. Peller, G. Winter, L. H. Lindner, and M. Hossann, "Thermosensitive liposomal drug delivery systems: State of the art review," *Int. J. Nanomed.*, vol. 9, pp. 4387–4398, Sep. 2014, doi: 10.2147/IJN.S49297.

[3] S. Mihcin and A. Melzer, "Principles of focused ultrasound," *Minimally Invasive Therapy Allied Technol.*, vol. 27, no. 1, pp. 41–50, 2018, doi: 10.1080/13645706.2017.1414063.

[4] Z. Izadifar, Z. Izadifar, D. Chapman, and P. Babyn, "An introduction to high intensity focused ultrasound: Systematic review on principles, devices, and clinical applications," *J. Clin. Med.*, vol. 9, no. 2, p. 460, Feb. 2020, doi: 10.3390/jcm9020460.

[5] Y.-H. Hsiao, S.-J. Kuo, H.-D. Tsai, M.-C. Chou, and G.-P. Yeh, "Clinical application of high-intensity focused ultrasound in cancer therapy," *J. Cancer*, vol. 7, no. 3, pp. 225–231, 2016, doi: 10.7150/jca.13906.

[6] R. M. S. Sigrist, J. Liau, A. E. Kaffas, M. C. Chammas, and J. K. Willmann, "Ultrasound elastography: Review of techniques and clinical applications," *Theranostics*, vol. 7, no. 5, pp. 1303–1329, 2017, doi: 10.7150/thno.18650.

[7] E. Boctor, M. Choti, E. Burdette, and R. J. Webster, "Three-dimensional ultrasound-guided robotic needle placement: An experimental evaluation," *Int. J. Med. Robot.*, vol. 4, no. 2, pp. 180–191, Jun. 2008, doi: 10.1002/rcs.184.

[8] C. Freschi, E. Troia, V. Ferrari, G. G. Megali, A. Pietrabissa, and F. Mosca, "Ultrasound guided robotic biopsy using augmented reality and human-robot cooperative control," in *Proc. Annu. Int. Conf. IEEE Eng. Med. Biol. Soc.*, 2009, pp. 5110–5113, doi: 10.1109/IEMBS.2009.5332720.

[9] M. Unger, J. Berger, B. Gerold, and A. Melzer, "Robot-assisted ultrasound-guided tracking of anatomical structures for the application of focused ultrasound," *Curr. Dir. Biomed. Eng.*, vol. 6, no. 3, pp. 123–126, Sep. 2020, doi: 10.1515/cdbme-2020-3032.

[10] N. Choong Kheng, N. Wan Sing, L. Phee, and C. Cheng, "A HIFU robot for transperineal treatment of prostate cancer," in *Proc. 2002 7th Int. Conf. Control. Autom. Robot. Vis. (ICARCV)*, vol. 2, pp. 560–565, doi: 10.1109/ICARCV.2002.1238485.

[11] S. Pather, B. L. Davies, and R. D. Hibberd, "The development of a robotic system for HIFU surgery applied to liver tumours," in *Proc. 2002 7th Int. Conf. Control. Autom. Robot. Vis. (ICARCV)*, pp. 572–577, doi: 10.1109/ICARCV.2002.1238487.

[12] Z. Qiu *et al.*, "The development of a robotic approach to therapeutic ultrasound," *J. Phys. Conf. Ser.*, vol. 181, no. 1, p. 012017, Aug. 2009, doi: 10.1088/1742-6596/181/1/012017.

[13] Y. T *et al.*, "A novel high intensity focused ultrasound robotic system for breast cancer treatment," *Med. Image Comput. Comput. Assisted Intervention*, vol. 16, no. Pt 3, pp. 388–395, 2013, doi: 10.1007/978-3-642-40760-4_49.

[14] T. Tang, T. Azuma, T. Iwahashi, H. Takeuchi, E. Kobayashi, and I. Sakuma, "A high-precision US-guided robot-assisted HIFU treatment system for breast cancer," *Engineering*, vol. 4, no. 5, pp. 702–713, 2018, doi: 10.1016/j.eng.2018.07.008.

[15] M. H. A. Groen *et al.*, "Safety and feasibility of arterial wall targeting with robot-assisted high intensity focused ultrasound: A preclinical study," *Int. J. Hyperthermia*, vol. 37, no. 1, pp. 903–912, Jan. 2020, doi: 10.1080/02656736.2020.1795278.

[16] N. Koizumi *et al.*, "A novel robust template matching method to track and follow body targets for NIUTS," in *Proc. IEEE Int. Conf. Robot. Autom.*, Sep. 2014, pp. 1929–1936, doi: 10.1109/ICRA.2014.6907114.

[17] L. Chanel, F. Nageotte, J. Vappou, J. Luo, L. Cuvillon, and M. de

Mathelin, "Robotized high intensity focused ultrasound (HIFU) system for treatment of mobile organs using motion tracking by ultrasound imaging: An in vitro study," in *Proc. 37th Annu. Int. Conf. IEEE Eng. Med. Biol. Soc.*, Nov. 2015, pp. 2571–2575, doi: 10.1109/EMBC.2015.7318917.

[18] C. Y. An, Y. L. Hsu, and C. S. Tseng, "An ultrasound-guided robotic HIFU ablation system with respiration induced displacement and time delay compensation," *J. Med. Biol. Eng.*, vol. 39, no. 5, pp. 796–805, doi: 10.1007/s40846-019-00463-0.

[19] S. Tognarelli, G. Ciuti, A. Diodato, A. Cafarelli, and A. Menciassi, "Robotic platform for high-intensity focused ultrasound surgery under ultrasound tracking: The FUTURA platform," *J. Med. Robot. Res.*, vol. 2, no. 3, p. 1740,010, 2017, doi: 10.1142/S2424905X17400104.

[20] S. C. Davies, A. L. Hill, R. B. Holmes, and P. C. Jackson, "Ultrasound quantitation of respiratory organ motion in the upper abdomen," *Brit. J. Radiol.*, vol. 67, no. 803, pp. 1096–1102, 1994, doi: 10.1259/0007-1285-67-803-1096.

[21] A. Diodato, A. Cafarelli, A. Schiappacasse, S. Tognarelli, G. Ciuti, and A. Menciassi, "Motion compensation with skin contact control for high intensity focused ultrasound surgery in moving organs," *Phys. Med. Biol.*, vol. 63, no. 3, p. 035017, 2018, doi: 10.1088/1361-6560/aa9c22.

[22] Z. Kalal, K. Mikolajczyk, and J. Matas, "Tracking-learning-detection," *IEEE Trans. Pattern Anal. Mach. Intell.*, vol. 34, no. 7, pp. 1409–1422, 2012, doi: 10.1109/TPAMI.2011.239.

[23] V. Simoni, A. Cafarelli, S. Tognarelli, and A. Menciassi, "Ex vivo assessment of multiple parameters in high intensity focused ultrasound," in *Proc. 40th Annu. Int. Conf. IEEE Eng. Med. Biol. Soc.*, Jul. 2018, pp. 5705–5708, doi: 10.1109/EMBC.2018.8513583.

[24] N. Koizumi and M. Mitsuishi, "A study on the construction methodology of remote ultrasound diagnosis system," *Robot. Soc. Japan*, vol. 25, no. 2, pp. 267–279, 2007, doi: 10.7210/jrsj.25.267.

[25] L. Morchi, A. Mariani, A. Diodato, S. Tognarelli, A. Cafarelli, and A. Menciassi, "Acoustic coupling quantification in ultrasound-guided focused ultrasound surgery: Simulation-based evaluation and experimental feasibility study," *Ultrasound Med. Biol.*, vol. 46, no. 12, pp. 3305–3316, 2020, doi: 10.1016/j.ultrasmedbio.2020.08.028.

[26] L. Morchi *et al.*, "A reusable thermochromic phantom for testing high intensity focused ultrasound technologies," in *Proc. 2021 IEEE 43th Annu. Int. Conf. IEEE Eng. Med. Biol. Soc. (EMBC)*, pp. 1431–1434, doi: 10.1109/EMBC46164.2021.9629845.

[27] A. J. Krafft *et al.*, "Robotically assisted focal spot scanning MRg-FUS: Initial in vivo experiments," in *Proc. IFMBE*, 2009, pp. 155–158, doi: 10.1007/978-3-642-03906-5_42.

[28] M. M. Swindle, A. C. Smith, and B. J. S. Hepburn, "Swine as models in experimental surgery," *J. Investigative Surg.*, vol. 1, no. 1, pp. 65–79, 1988, doi: 10.3109/08941938809141077.

Andrea Mariani, The BioRobotics Institute and Department of Excellence in Robotics and AI, Sant'Anna School of Advanced Studies, Pisa, 56025, Italy. Email: andrea.mariani@santannapisa.it.

Laura Morchi, The BioRobotics Institute and Department of Excellence in Robotics and AI, Sant'Anna School of Advanced Studies, Pisa, 56025, Italy. Email: laura.morchi@santannapisa.it.

Alessandro Diodato, The BioRobotics Institute and Department of Excellence in Robotics and AI, Sant'Anna School of Advanced Studies, Pisa, 56025, Italy. Email: alessandro.diodato@alumni.sssup.it.

Selene Tognarelli, The BioRobotics Institute and Department of Excellence in Robotics and AI, Sant'Anna School of Advanced Studies, Pisa, 56025, Italy. Email: selene.tognarelli@santannapisa.it.

Arianna Menciassi, The BioRobotics Institute and Department of Excellence in Robotics and AI, Sant'Anna School of Advanced Studies, Pisa, 56025, Italy. Email: arianna.menciassi@santannapisa.it.